

Size and transparency influence diel vertical migration patterns in copepods.

Alex Barth

Rod Johnson

Joshua Stone

27 Mar 2023

1 Abstract

Diel vertical migration (DVM) is a widespread phenomenon in aquatic environments. The primary hypothesis explaining DVM is the visual predator evasion hypothesis, which suggests that zooplankton migrate to deeper waters to avoid detection during daylight. However, visual risk also depends on a copepod's morphology. In this study, we investigate hypotheses related to morphology and DVM: (H1) size increases visual risk and will increase DVM depth and (H2) copepod transparency will reduce visual risk and thus reduce DVM depth. In-situ Copepod images were collected across several cruises in the Sargasso Sea using an Underwater Vision Profiler 5. Copepod morphology was characterized from these images and a dimension reduction approach. The results show a clear relationship in which larger copepods have a larger DVM signal. Darker copepods also have a larger DVM signal, however only amongst the largest group of copepods. This suggests multiple morphological traits influence copepod DVM behavior.

18 **2 *Scientific Significance Statement***

19 Diel Vertical Migration is a widespread phenomenon across marine and freshwater systems.
20 The predator evasion hypothesis suggests that DVM occurs as zooplankton attempt to escape
21 visual predators. Yet, DVM itself is a costly and risky behavior. Thus, DVM should only
22 occur when visual risk is high. Several studies have shown that copepod size influences the
23 magnitude of DVM. However, an individual's visual risk may include traits beyond simply
24 size. In this study, we utilize an in-situ imaging tool to reveal how copepod morphological
25 traits influence DVM. Our findings show that both size and transparency influence DVM. This
26 finding highlights that DVM is a complex behavior driven by copepod traits. Furthermore,
27 this study exemplifies the ability of new technology to draw insights into plankton ecology.

28 **3 Introduction**

29 Diel vertical migration (DVM) is a wide spread phenomena with large consequences in ocean
30 ecosystems. DVM is the process of pelagic organisms vertically moving in the water column
31 on a daily basis, often travelling dozens to hundreds of meters (Bianchi and Mislan 2016).
32 This large-scale event occurs across many taxa, from plankton to fish (Brierley 2014). How-
33 ever, DVM is particularly notable in zooplankton communities, whose migrations contribute
34 substantially to biogeochemical cycles (Steinberg and Landry 2017; Archibald et al. 2019;
35 Siegel et al. 2023). Zooplankton communities, largely dominated by copepods (Turner 2004),
36 will feed in surface layers of the ocean at night then migrate into deeper waters during day-

37 time. Through this movement, copepods actively transport carbon to depth. Additionally,
38 Kelly et al. (2019) described zooplankton DVM to be a major component of mesopelagic food
39 webs. Thus to understand pelagic food webs and nutrient cycles, it is critically important to
40 understand the drivers of DVM.

41 Predominantly, zooplankton DVM is the movement from deep waters at daytime to shallower
42 waters at night (Hays 2003; Bianchi and Mislan 2016). The leading explanation for this
43 pattern is the predator-avoidance hypothesis (Bandara et al. 2021). This hypothesis posits
44 zooplankton evacuate the sunlit surface to evade visual predators then ascend at night to
45 feed. However, the massive migration undertaken by these copepods is energetically expensive
46 (Maas et al. 2018; Robison et al. 2020). Therefore, the visual predator evasion hypothesis
47 implies that DVM is a result of visual risk exceeding migration costs. However, a copepod's
48 visual risk to a visual predator depends on morphological features (Aksnes and Utne 1997).
49 Notably a copepod's size can increase visual detection. Several studies have documented that
50 copepod size influences DVM magnitude (Hays et al. 1994; Aarflot et al. 2019). Presumably, a
51 copepod's transparency will also influence DVM. Hays et al. (1994) reported that pigmentation
52 explained variation in DVM frequency. However, few other studies have investigated this at
53 length. One barrier to studying a relationship between copepod morphology and DVM is the
54 difficulty of accurately recording traits.

55 In-situ imaging tools offer great potential to better describe copepod DVM. By directly ob-
56 serving copepods, new insights into their behavior and traits can be resolved (Ohman 2019).
57 For example, Whitmore and Ohman (2021) used an in-situ imaging device to describe a rela-

58 tionship between copepod abundance with a particulate field rather than chlorophyll-a. Such
59 findings are facilitated by the fact imagery data records an individual's exact position. Ad-
60 ditionally, a copepod's true appearance can be documented whereas net-collected organisms
61 are often physically deformed or lacking color due to decomposition or preservation. Some
62 studies have noted a copepod DVM with in-situ imagery data (Pan et al. 2018; Whitmore
63 and Ohman 2021). However, direct tests of DVM-related hypotheses with such data have not
64 been conducted.

65 In this study, we utilized in-situ imaging to evaluate how copepod morphological traits influ-
66 ence patterns. We specifically test the hypotheses that, (H1) size increases visual risk and
67 will increase DVM magnitude and (H2) copepod transparency will reduce visual risk and thus
68 reduce DVM. If these morphologically based hypotheses are true, then the larger and darker
69 copepods will have the largest DVM signals.

70 **4 Methods**

71 **4.1 CTD profiles and UVP imaging of copepods**

72 Data were collected aboard the R/V Atlantic Explorer in collaboration with the Bermuda
73 Atlantic Time-series Study (BATS) (Steinberg et al. 2001). In-situ images of plankton were
74 acquired using an Underwater Vision Profiler (UVP5) (Picheral et al. 2010). The original
75 sampling methodology and instrument specification followed details described in Barth and
76 Stone (2022). The UVP was attached to the CTD rosette and deployed regularly on cruises

77 to the Sargasso Sea from June 2019 - December 2021. Typical monthly cruises included ~13
78 profiles with average descents to 1200m (Supplemental Figure 1). In this study, we investigated
79 general trends in DVM by pooling together casts across multiple cruises. This approach is
80 necessitated by the small sampling volume of the UVP and low abundance of plankton which
81 requires aggregation of data to resolve trends (Barth and Stone 2022). While there was
82 some variation between cruises (Supplemental Figure 2), this oligotrophic system is relatively
83 consistent across seasons. Additionally, every cruise had an approximately equal number of
84 day and night casts. Profiles were assigned to be day or night based on locally calculated
85 nautical dawn and nautical dusk times using the R package `suncalc` 0.5.1.

86 The UVP records images of large particles ($>600\mu\text{m}$ ESD). However, living particles are not
87 reliably identifiable below 0.9 mm (Barth and Stone 2022). All recorded images were processed
88 using Zooprocess (Gorsky et al. 2010), which provides several metrics related to size, grey
89 value, and shape complexity. These features were then used to automatically sort images using
90 Ecotaxa (Picheral et al.). All images were manually verified by the same trained taxonomist.
91 In total, 294,913 images were recorded. Of these, 85.2% were images of debris or artefacts.
92 The smallest identified copepod was 0.940mm ESD and the largest was 5.904mm ESD. Across
93 all casts, copepods were the most common organism, composing 58.7% of all identified, living
94 particles. In total, there were 4151 individual copepods images.

95 4.2 Morphological Grouping

96 Zooprocess measures and collects several morphologically relevant parameters. To create rel-
97 evant groups of copepods, a dimension reduction approach was used. Similar methods have
98 been successfully utilized to provide novel insights to marine snow (Trudnowska et al. 2021),
99 copepod dynamics in the Arctic (Vilgrain et al. 2021), and temporal trends in phytoplankton
100 communities (Sonnet et al. 2022). First, 18 morphologically relevant parameters were selected
101 to be included in a principal Components Analysis (PCA), following (Vilgrain et al. 2021).
102 Parameters can be described as relating to size (e.g. major axis, feret diameter, ESD), grey
103 intensity (e.g. mean grey value at 625nm wavelength light), shape (e.g. elongation, symmetry),
104 and shape complexity (e.g. fractal dimension). The PCA was weighted by the volume sampled
105 in a 1-m depth bin for each observation. This approach provides a correction for the UVP's
106 variable descent speed which can cause duplicate imaging of individuals. While this phenomena
107 has a minor impact on overall results (Barth and Stone 2022), we used the weighted approach
108 to assure that no individual features were overrepresented. All morphological descriptors were
109 scaled and centered prior to inclusion in the analysis. The model was constructed using the R
110 package **FactoMineR** 2.7. principal components were deemed to be significant if their eigen-
111 values were greater than 1. This approach yielded 4 PCs which described 87.3% of the total
112 variation in morphological parameters, with 34.5% and 26.5% in the first two components
113 respectively. This four principal component space provides a “morphospace” to characterize
114 copepods.

115 To address our morphology-DVM hypotheses, we constructed discrete morphological groups

116 based on the first two principal components. Groups along each of the principal components
117 were defined as low (below 25th percentile), mid (25th-75th percentile) and high (greater than
118 75th percentile). To address the size-dependent hypothesis (H1), groups were assigned as low,
119 mid, or high along PC1. Then to assess if color/transparency was a secondary factor (H2),
120 within each PC1 group, PC2 groups were constructed as low, mid, or high. In total, this
121 created 9 groups (e.g. Low PC1-Low PC2, Low P1-mid PC2, etc).

122 **4.3 Copepod vertical structure & DVM**

123 **4.3.1 Vertical distribution of copepods**

124 Copepods in this system are well documented to undergo DVM (Steinberg et al. 2000; Schnet-
125 zer and Steinberg 2002; Maas et al. 2018). However, there have not been direct measurements
126 of DVM with in-situ imaging data. First, to assess which portion of the water column cope-
127 pods were utilizing for DVM, we visualized the average vertical structure. The concentrations
128 of each morphological group (based on PC1 and PC2) were calculated in 20m depth bins for
129 each UVP profile. These binned-profiles were then averaged together based on time of day.

130 **4.3.2 Weighted mean depth variability**

131 Weighted mean depth (WMD) is a common metric to describe vertical structure and DVM in
132 zooplankton (Ohman et al. 2002; Ohman and Romagnan 2016; Aarflot et al. 2019). However,
133 with in-situ imagery, this approach presents a few challenges. WMD cannot be calculated

134 individually for each profile then averaged because each profile had a different descent depth.
 135 Additionally, the small and uneven sampling volume of the UVP can make single casts too
 136 variable to reliably resolve abundance. Yet, understanding variation around the WMD is nec-
 137 essary to compare DVM strength across groups. Here, we introduce a depth-bin constrained
 138 bootstrap approach to define WMD with a 95% confidence interval. To do this, the concentra-
 139 tion of each group, was calculated in 20m depth bins for each profile. Then all profiles from
 140 the same time of day were ‘pooled’. This provides a distribution of concentrations in each
 141 depth-bin. Traditional bootstrapping randomly samples, with replacement, all observations.
 142 With vertically structured data however, full random sampling would bias estimates towards
 143 the surface. To avoid this, samples were “bin-constrained” such that for each iteration, a
 144 random observation was sampled within each depth bin, then replaced for the next iteration.
 145 A maximum depth was set to 600m based on observations of vertical profiles which indicated
 146 this to be the maximum point of day/night differences. This approach effectively created a
 147 random profile by resampling a concentration, $conc^*$, from each depth bin, d . This profile then
 148 was used to calculate a bootstrapped weighted mean depth, WMD^* . This was done for each
 149 morphological group g , at each time of day t .

$$WMD_{g,t}^* = \sum_i^{N=60} \frac{d_i(conc_{i,g,t}^*)}{\sum_i^{N=60} conc_{i,g,t}^*}$$

150 The distribution of $WMD_{g,t}^*$ then was used to calculate a bootstrapped mean and 95% con-
 151 fidence interval. The 95% CIs could be compared between times of day and morphological
 152 groups to assess the strength of DVM. Using PC1 to assess size, the WMD was compared

between the three PC1-groups by percentile level. Then to assess the effect of transparency the WMD was compared between PC2-groups within each PC1-grouping. A larger signal of DVM would be evident by a clearly deeper (non-overlapping 95% CI) daytime WMD.

4.4 Data availability

All data and code are made available via (https://github.com/TheAlexBarth/DVM_Migration-Morphology). All supplemental figures, tables, and analyses are available at (https://thealexbarth.github.io/DVM_Migration-Morphology).

5 Results

5.1 Morphological Groups

The PCA revealed four major axis of variability (Figure 1). The first axis (PC1, 34.23% of variability) was largely explained by increasing values related to size, such as perimeter (loading score = 0.927) and feret diameter (loading score = 0.910). The second axis (PC2, 27.24% of variability) can be interpreted as a gradient of transparent to dark individuals. PC2 was largely anticorrelated with mean grey value (higher values indicate a more transparent individual) (loading score = -0.920). As noted in the methods, PC3 and PC4 were both related to the orientation of the copepod and the appendage visibility respectively (Supplemental Figure 3).

The morphological groupings were assigned along PC1 as low, mid and high. Then along PC2, groups were assigned within each PC1-group (Figure 1). To confirm the morphospace grouping

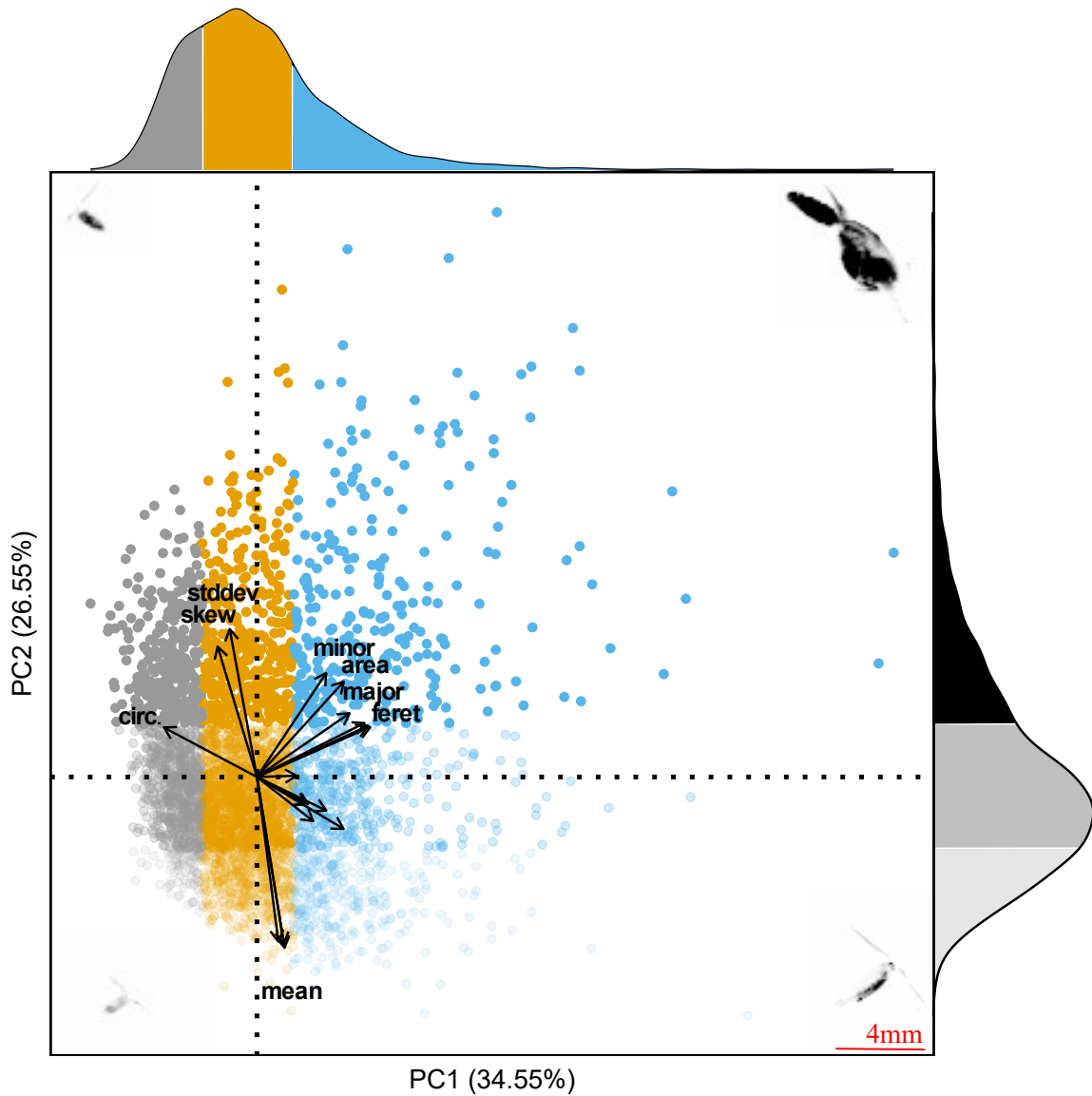


Figure 1: First two principal components of the morphospace. Proportion of variance explained by the two axis is . Each point represents an individual copepod. The color and transparency of each point corresponds to the morphological groups based on percentile along each axis. Marginal distribution display the proportion of observations in each group. Representative vignettes of copepods are shown in the corners corresponding to their place in the morphospace. 4mm scale bar in the bottom right is shown for the vignettes.

171 resulted in ecologically relevant categories, the morphological groups were compared against
172 known copepod metrics. Across all PC1-groups, there was a clear difference in feret diameter.
173 The median feret diameter of the low group was 1.97mm. The median feret diameter of the
174 mid and high groups were 2.84mm and 4.83mm, respectively (Figure 2A). All groups were
175 significantly different from one another (Dunn Kruskall-Wallace test, $p < 0.001$). PC2 groups
176 as a whole were also significantly different from one another (Dunn Kruskall-wallace test, $p <$
177 0.001). However, within each PC2-group, there was a clear tendency for larger copepods (high
178 PC1 group) to be more transparent (Figure 2B).

179 **5.2 Vertical Profiles of Morphological Groups**

180 For all groups, the 20m-binned profiles show a notable structure. While copepods were ob-
181 served throughout the mesopelagic (Supplemental Figure 4), the majority of day/night differ-
182 ences were observed above 600m (Figure 3). For all morphological groups, there was a peak in
183 nighttime concentration in the lower epipelagic (50m-200m). Similarly, there was a decrease
184 in average daytime concentration over the same region. This pattern is particularly apparent
185 for the groups which are mid and high on both PCs (Figure 3B, C, E, F). Across all groups,
186 both average daytime and nighttime concentration were low in the upper mesopelagic (200m-
187 300m). Then, there was a peak in average daytime concentration in the depth bins in the
188 mid-mesopelagic (400m-600m).

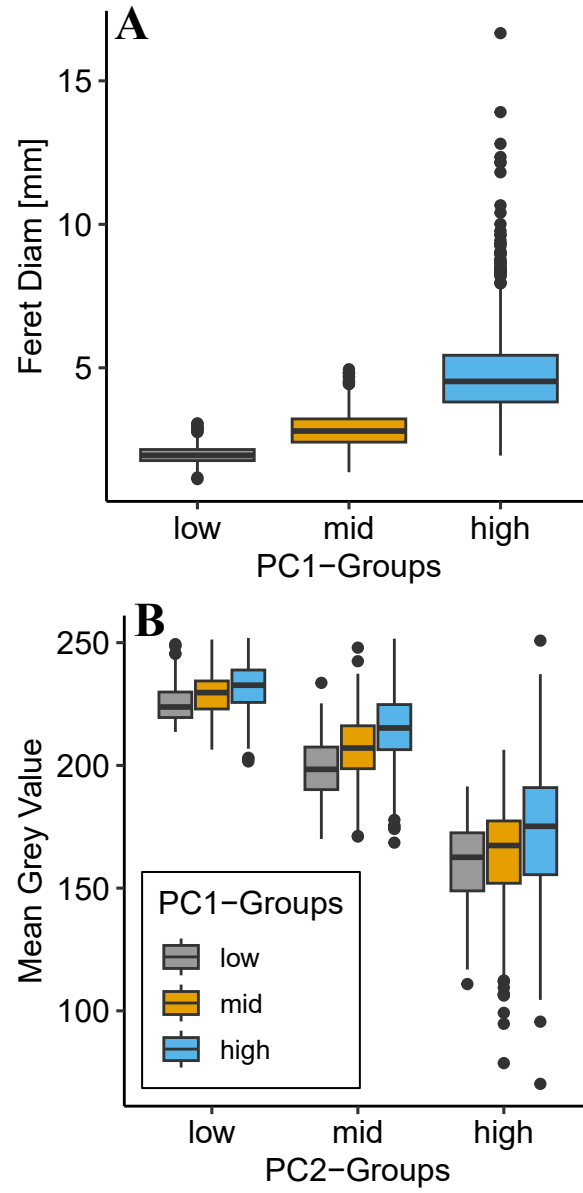


Figure 2: Comparison of morphological groups to relevant parameters. Groups were constructed along principal components with low as below 25th percentile, mid as 25th-50th percentile, and high as above 75th percentile. (A) PC1 groups are significantly different along feret diameter and display a clear trend for size. (B) PC2 groups are significantly different in terms of mean grey value. Note that a low mean grey value indicates a darker copepod.

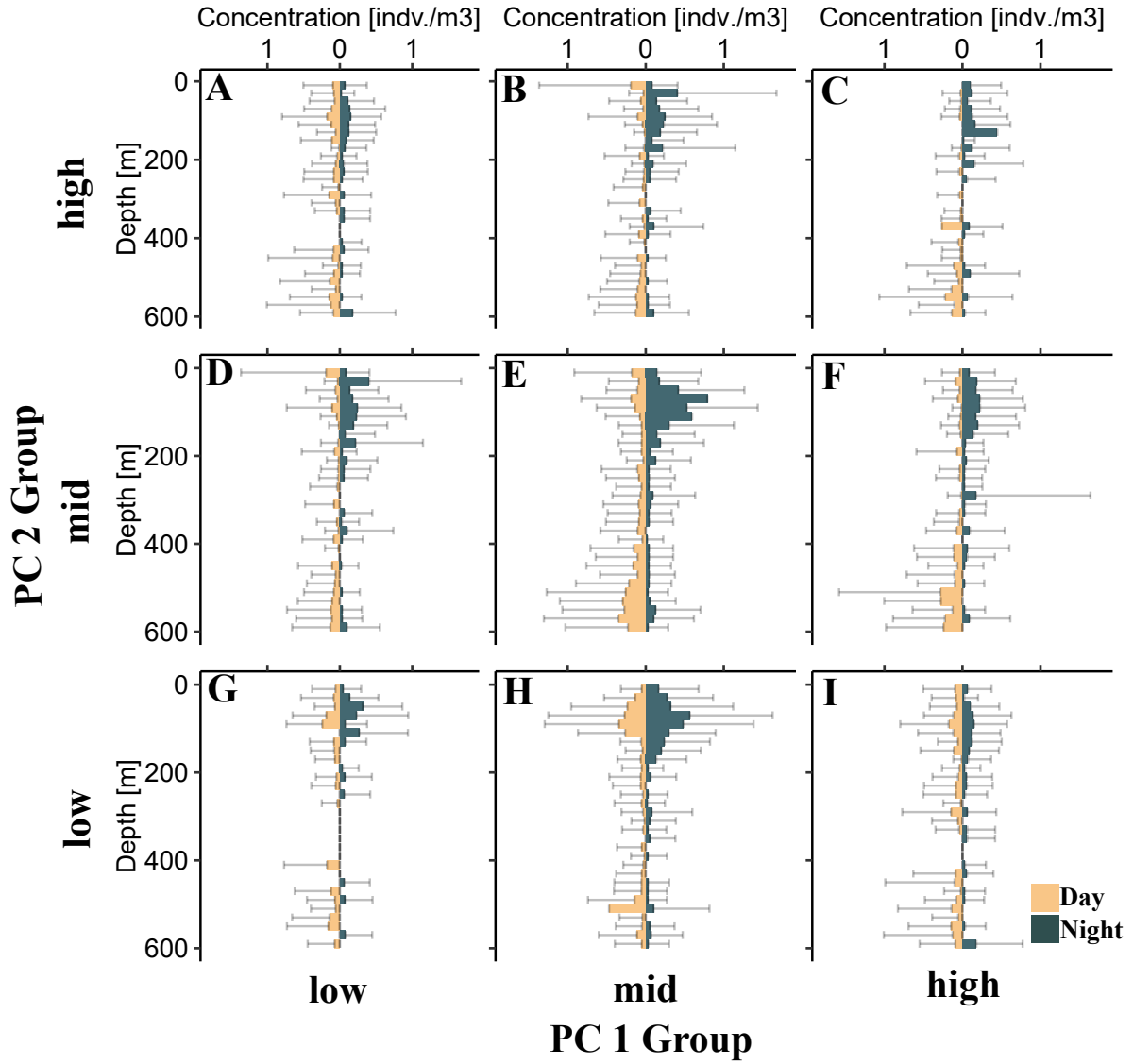


Figure 3: Average vertical profile of different copepod morphological groups. Bars display average concentration in a 20m depth bin. On each panel, left-side bars (tan) correspond to daytime while right-side (teal) bars correspond to nighttime. Standard deviation is shown for each 20m depth bin. Each panel corresponds to a morphological group along PC1 (size axis) and PC2 (transparency axis). (A) low PC1, high PC2; (B) mid PC1, high PC2; (C) high PC1, high PC2; (D) low PC1, mid PC2; (E) mid PC1, mid PC2; (F) high PC1, mid PC2; (G) low PC1, low PC2; (H) mid PC1, low PC2; (I) high PC1, low PC2

5.3 Weighted mean depth analysis

The bin-constrained bootstrap approach provided a direct method to compare DVM between groups. Size (PC1) had a clear effect on DVM magnitude. First, for all PC1 groups, daytime WMD 95% bootstrapped confidence intervals (95% CIs) were deeper and non-overlapping with the nighttime 95% CIs (Figure 4). This indicates a clear DVM pattern. However, the differences in day and night CIs varied between morphological groups. All PC1 groups had a similar, overlapping nighttime 95% CI in the lower epipelagic (~145m - ~200m). However, there was a clear difference in the depth of the daytime 95% CIs. The small (low PC1) group had the shallowest 95% CI (235.2m-296.0m). The mid PC1 group's daytime 95% CI was slightly deeper (309.0m-347.3m). The large (high PC1) group daytime 95% CI was even lower (352.3m-405.0m).

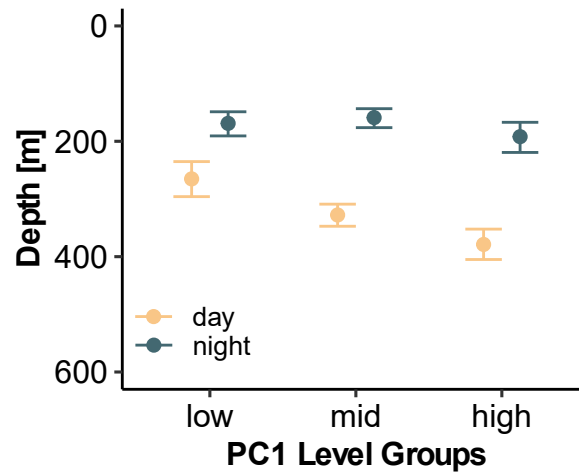


Figure 4: Mean bootstrapped weighted mean depth and 95% confidence intervals for copepods of different morphological groups. Low, mid, and high groups correspond to the different percentiles along PC1 from the morphospace. PC1 largely is explained by size metrics, with higher scores indicating a larger copepod.

When considering the influence of transparency (PC2) on DVM magnitude, we compared PC2 groups within their PC1 grouping. This approach was warranted because of the tendency for size to have a slight effect on transparency (Figure 2). At this level of comparison, there were several notable trends. For the smaller copepods (low PC1), once the data were split into PC2 groups, the wider 95% CIs indicate little to no DVM signal. Generally, the daytime 95% CIs and nighttime 95% CIs are overlapping or near-overlapping (Figure 5A). With mid sized copepods, there was a clear DVM signal. However, all PC2 groups appeared to have a similar DVM magnitude with each group's daytime 95% CIs overlapping with each other (Figure 5B). There was a difference in DVM magnitude across PC2 groups within the largest copepods. The more transparent copepods (low PC2 group) showed no DVM signal, with a shallow daytime WMD. However, the darker copepods (mid and high PC2 groups) had deeper daytime WMDs (Figure 5c).

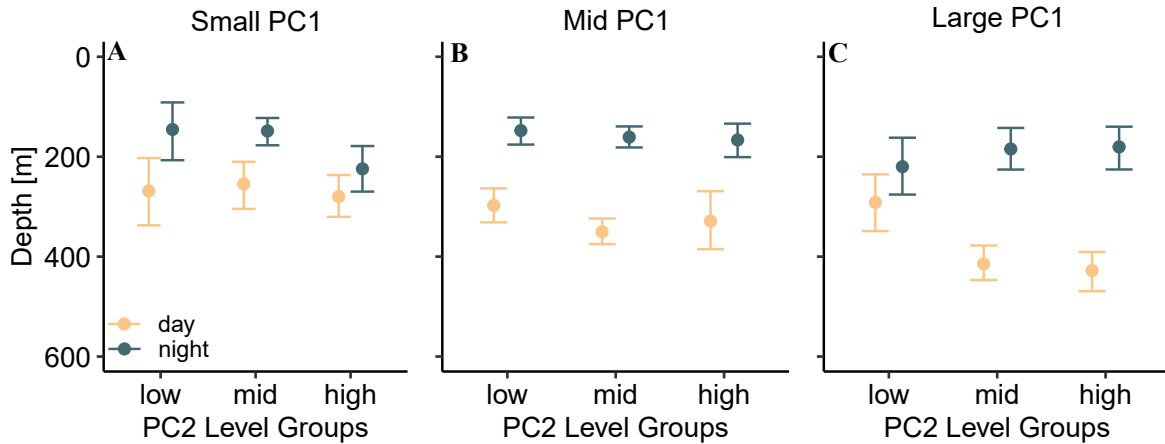


Figure 5: Mean bootstrapped weighted mean depth and 95% confidence intervals shown by copepod morphological groups along PC2 (transparency). Each panel represents a different size group of copepods (PC1 groups).

6 Discussion

6.1 Copepod morphospace

In this study, we built on methods for describing morphospaces from similar in-situ imaging studies (Vilgrain et al. 2021; Trudnowska et al. 2021; Sonnet et al. 2022). The PCA-defined morphospace with the present data aligns well with the prior applications. Interestingly, the proportion of variation explained by each axis in the morphospace defined on Arctic copepods by Vilgrain et al. (2021) is extremely similar to the morphospace axes in this study. It is possible that this is an artifact of the similarity of input data. Given the UVP has a limited range of observable size classes (Picheral et al. 2010), only copepods above a certain size were fed into both PCAs. Nonetheless, it is striking that the two morphospaces are similar considering the vastly different community compositions between the Arctic ocean and subtropical gyres (Soviadan et al. 2022).

6.2 Morphology and DVM

The pattern of DVM described in this study is consistent with the general nighttime ascent DVM pattern (Bianchi and Mislán 2016; Bandara et al. 2021). The average vertical profiles display a clear day/night difference (Figure 3). In each 20m depth bin, there was large variation, often exceeding the average concentration. This large variation however, was expected. There can be considerable variation between UVP estimates of zooplankton abundance (Barth and Stone 2022). Additionally, in this study we pooled casts across multiple seasons. Variability

231 in copepod DVM has been described across seasons (Whitmore and Ohman 2021). While
232 seasonal variability in DVM is in an interesting question in the Sargasso Sea, the nature of our
233 dataset did not lend itself to this investigation. However, despite the need to pool UVP casts
234 across cruises, the signal of DVM was still observable. Previous studies using in-situ imaging
235 have also noted a signal of DVM with copepods (Pan et al. 2018; Whitmore and Ohman 2021).
236 Yet due to small and uneven sampling, it can be a challenge to quantify DVM using in-situ
237 imaging. As presented in this paper, bin-constrained bootstrapping offers a robust method to
238 quantify WMD and investigate DVM hypotheses.

239 Copepod size had a clear effect in which larger copepods migrated further. This finding
240 is consistent with several studies which have documented a size-dependent relationship for
241 copepod DVM (Ohman and Romagnan 2016; Aarflot et al. 2019; Pinti et al. 2019). Ohman
242 and Romagnan (2016) noted that moderate-size copepods had the largest migrations. While
243 this may seem contradictory to the present study, the difference between study systems needs
244 be taken into account. The copepods described in the large (high PC1) group had a mean feret
245 diameter of nearly 5mm. Conversely, in Ohman and Romagnan (2016)’s study the “moderate”
246 copepods ranged from 4mm-6mm. An effect of transparency on copepod DVM was only
247 observed in the large copepod group. The large but more transparent copepods (low PC2, high
248 PC1) did not have a detectable DVM signal. Yet the darker copepods (mid and high PC2) had
249 a large DVM signal. Hays (2003) described that copepod pigmentation could explain increased
250 DVM with small ($<1\text{mm}$) copepods. The lack of a transparency effect for the mid- and low
251 PC1 groups in our study is surprising. One possibility is that the small, transparent copepods

were not well sampled by the UVP (Figure 2). Alternatively, some copepods which do not migrate may have pigmentation to avoid damage from UV radiation. The grey-value recorded in UVP-imaged copepods can be indicative of many features beyond simply pigmentation, notably egg-sacs and gut contents (Vilgrain et al. 2021). Such characteristics vary much more between individuals and can have varied influences on DVM (PEARRE Jr. 2003). Thus the relationship between color and DVM is the result of a delicate balance of minimizing multiple ecological and biological risks (Hansson 2004; Hylander et al. 2014). While well documented, predator avoidance may not always be the primary selective pressure on copepod traits. For example, if the costs of migration are too large for some copepods, they will remain near the surface. However, these copepods then are exposed to UV light and may increase pigmentation to reduce damage. Overall, our results reveal a complex dynamic between copepod traits and DVM behavior. Additionally, we show that in-situ imaging systems can be used to investigate ecological hypotheses.

References

- Aarflot, J. M., D. L. Aksnes, A. F. Opdal, H. R. Skjoldal, and Ø. Fiksen. 2019. Caught in broad daylight: Topographic constraints of zooplankton depth distributions. *Limnology and Oceanography* **64**: 849–859. doi:[10.1002/lno.11079](https://doi.org/10.1002/lno.11079)
- Aksnes, D. L., and A. C. W. Utne. 1997. A revised model of visual range in fish. *Sarsia* **82**: 137–147. doi:[10.1080/00364827.1997.10413647](https://doi.org/10.1080/00364827.1997.10413647)
- Archibald, K. M., D. A. Siegel, and S. C. Doney. 2019. Modeling the Impact of Zooplank-

272 ton Diel Vertical Migration on the Carbon Export Flux of the Biological Pump. *Global*
 273 *Biogeochemical Cycles* **33**: 181–199. doi:[10.1029/2018GB005983](https://doi.org/10.1029/2018GB005983)

274 Bandara, K., Ø. Varpe, L. Wijewardene, V. Tverberg, and K. Eiane. 2021. Two hun-
 275 dred years of zooplankton vertical migration research. *Biological Reviews* **96**: 1547–1589.
 276 doi:[10.1111/brv.12715](https://doi.org/10.1111/brv.12715)

277 Barth, A., and J. Stone. 2022. [Comparison of an in situ imaging device and net-based method](#)
 278 [to study mesozooplankton communities in an oligotrophic system.](#) *Frontiers in Marine*
 279 *Science* **9**.

280 Bianchi, D., and K. a. S. Mislan. 2016. Global patterns of diel vertical migration
 281 times and velocities from acoustic data. *Limnology and Oceanography* **61**: 353–364.
 282 doi:[10.1002/lno.10219](https://doi.org/10.1002/lno.10219)

283 Brierley, A. S. 2014. Diel vertical migration. *Current Biology* **24**: R1074–R1076.
 284 doi:[10.1016/j.cub.2014.08.054](https://doi.org/10.1016/j.cub.2014.08.054)

285 Gorsky, G., M. D. Ohman, M. Picheral, and others. 2010. Digital zooplankton image anal-
 286 ysis using the ZooScan integrated system. *Journal of Plankton Research* **32**: 285–303.
 287 doi:[10.1093/plankt/fbp124](https://doi.org/10.1093/plankt/fbp124)

288 Hansson, L.-A. 2004. Plasticity in Pigmentation Induced by Conflicting Threats from Preda-
 289 tion and Uv Radiation. *Ecology* **85**: 1005–1016. doi:[10.1890/02-0525](https://doi.org/10.1890/02-0525)

290 Hays, G. C. 2003. [A review of the adaptive significance and ecosystem consequences of zoo-](#)
 291 [plankton diel vertical migrations.](#) Springer Netherlands. 163–170.

292 Hays, G. C., C. A. Proctor, A. W. G. John, and A. J. Warner. 1994. Interspecific differences
 293 in the diel vertical migration of marine copepods: The implications of size, color, and mor-

294 phology. *Limnology and Oceanography* **39**: 1621–1629. doi:[10.4319/lo.1994.39.7.1621](https://doi.org/10.4319/lo.1994.39.7.1621)

295 Hylander, S., J. C. Grenvald, and T. Kiørboe. 2014. Fitness costs and benefits of ultra-
 296 violet radiation exposure in marine pelagic copepods. *Functional Ecology* **28**: 149–158.
 297 doi:[10.1111/1365-2435.12159](https://doi.org/10.1111/1365-2435.12159)

298 Kelly, T. B., P. C. Davison, R. Goericke, M. R. Landry, M. D. Ohman, and M. R. Stukel. 2019.
 299 [The importance of mesozooplankton diel vertical migration for sustaining a mesopelagic](#)
 300 [food web](#). *Frontiers in Marine Science* **6**.

301 Maas, A. E., L. Blanco-Bercial, A. Lo, A. M. Tarrant, and E. Timmins-Schiffman. 2018. Vari-
 302 ations in copepod proteome and respiration rate in association with diel vertical migration
 303 and circadian cycle. *The Biological Bulletin* **235**: 30–42. doi:[10.1086/699219](https://doi.org/10.1086/699219)

304 Ohman, M. D. 2019. A sea of tentacles: optically discernible traits resolved from planktonic
 305 organisms in situ H. Browman [ed.]. *ICES Journal of Marine Science* **76**: 1959–1972.
 306 doi:[10.1093/icesjms/fsz184](https://doi.org/10.1093/icesjms/fsz184)

307 Ohman, M. D., and J.-B. Romagnan. 2016. Nonlinear effects of body size and optical at-
 308 tenuation on Diel Vertical Migration by zooplankton. *Limnology and Oceanography* **61**:
 309 765–770. doi:[10.1002/lno.10251](https://doi.org/10.1002/lno.10251)

310 Ohman, M. D., J. A. Runge, E. G. Durbin, D. B. Field, and B. Niehoff. 2002. On birth and
 311 death in the sea. *Hydrobiologia* **480**: 55–68. doi:[10.1023/A:1021228900786](https://doi.org/10.1023/A:1021228900786)

312 Pan, J., F. Cheng, and F. Yu. 2018. [The diel vertical migration of zooplankton in the hypoxia](#)
 313 [area observed by video plankton recorder](#). *IJMS Vol.47(07)* [July 2018].

314 PEARRE Jr., S. 2003. Eat and run? The hunger/satiation hypothesis in verti-
 315 cal migration: history, evidence and consequences. *Biological Reviews* **78**: 1–79.

doi:[10.1017/S146479310200595X](https://doi.org/10.1017/S146479310200595X)

Picheral, M., S. Colin, and J.-O. Irisson. [EcoTaxa, a tool for the taxonomic classification of images.](#)

Picheral, M., L. Guidi, L. Stemann, D. M. Karl, G. Iddaoud, and G. Gorsky. 2010. The Underwater Vision Profiler 5: An advanced instrument for high spatial resolution studies of particle size spectra and zooplankton. *Limnology and Oceanography: Methods* **8**: 462–473. doi:[10.4319/lom.2010.8.462](https://doi.org/10.4319/lom.2010.8.462)

Pinti, J., T. Kiørboe, U. H. Thygesen, and A. W. Visser. 2019. Trophic interactions drive the emergence of diel vertical migration patterns: A game-theoretic model of copepod communities. *Proceedings of the Royal Society B: Biological Sciences* **286**: 20191645. doi:[10.1098/rspb.2019.1645](https://doi.org/10.1098/rspb.2019.1645)

Robison, B. H., R. E. Sherlock, K. R. Reisenbichler, and P. R. McGill. 2020. [Running the gauntlet: Assessing the threats to vertical migrators.](#) *Frontiers in Marine Science* **7**.

Schnetzer, A., and D. K. Steinberg. 2002. Active transport of particulate organic carbon and nitrogen by vertically migrating zooplankton in the Sargasso Sea. *Marine Ecology Progress Series* **234**: 71–84. doi:[10.3354/meps234071](https://doi.org/10.3354/meps234071)

Siegel, D. A., T. DeVries, I. Cetinić, and K. M. Bisson. 2023. Quantifying the ocean’s biological pump and its carbon cycle impacts on global scales. *Annual Review of Marine Science* **15**: null. doi:[10.1146/annurev-marine-040722-115226](https://doi.org/10.1146/annurev-marine-040722-115226)

Sonnet, V., L. Guidi, C. B. Mouw, G. Puggioni, and S.-D. Ayata. 2022. Length, width, shape regularity, and chain structure: time series analysis of phytoplankton morphology from imagery. *Limnology and Oceanography* **67**: 1850–1864. doi:[10.1002/lno.12171](https://doi.org/10.1002/lno.12171)

338 Soviadan, Y. D., F. Benedetti, M. C. Brandão, and others. 2022. Patterns of mesozooplankton
 339 community composition and vertical fluxes in the global ocean. *Progress in Oceanography*
 340 **200**: 102717. doi:[10.1016/j.pocean.2021.102717](https://doi.org/10.1016/j.pocean.2021.102717)

341 Steinberg, D. K., C. A. Carlson, N. R. Bates, S. A. Goldthwait, L. P. Madin, and A. F. Michaels.
 342 2000. Zooplankton vertical migration and the active transport of dissolved organic and
 343 inorganic carbon in the Sargasso Sea. *Deep Sea Research Part I: Oceanographic Research*
 344 *Papers* **47**: 137–158. doi:[10.1016/S0967-0637\(99\)00052-7](https://doi.org/10.1016/S0967-0637(99)00052-7)

345 Steinberg, D. K., C. A. Carlson, N. R. Bates, R. J. Johnson, A. F. Michaels, and A. H.
 346 Knap. 2001. Overview of the US JGOFS Bermuda Atlantic Time-series Study (BATS):
 347 a decade-scale look at ocean biology and biogeochemistry. *Deep Sea Research Part II:*
 348 *Topical Studies in Oceanography* **48**: 1405–1447. doi:[10.1016/S0967-0645\(00\)00148-X](https://doi.org/10.1016/S0967-0645(00)00148-X)

349 Steinberg, D. K., and M. R. Landry. 2017. Zooplankton and the ocean carbon cycle. *Annual*
 350 *Review of Marine Science* **9**: 413–444. doi:[10.1146/annurev-marine-010814-015924](https://doi.org/10.1146/annurev-marine-010814-015924)

351 Trudnowska, E., L. Lacour, M. Ardyna, A. Rogge, J. O. Irisson, A. M. Waite, M. Babin, and
 352 L. Stemann. 2021. Marine snow morphology illuminates the evolution of phytoplankton
 353 blooms and determines their subsequent vertical export. *Nature Communications* **12**: 2816.
 354 doi:[10.1038/s41467-021-22994-4](https://doi.org/10.1038/s41467-021-22994-4)

355 Turner, J. 2004. The importance of small planktonic copepods and their roles in pelagic marine
 356 food webs,.

357 Vilgrain, L., F. Maps, M. Picheral, M. Babin, C. Aubry, J.-O. Irisson, and S.-D. Ayata.
 358 2021. Trait-based approach using in situ copepod images reveals contrasting ecological
 359 patterns across an Arctic ice melt zone. *Limnology and Oceanography* **66**: 1155–1167.

360 doi:[10.1002/lno.11672](https://doi.org/10.1002/lno.11672)

361 Whitmore, B. M., and M. D. Ohman. 2021. Zooglider-measured association of zooplank-
362 ton with the fine-scale vertical prey field. *Limnology and Oceanography* **66**: 3811–3827.

363 doi:[10.1002/lno.11920](https://doi.org/10.1002/lno.11920)